Biomimicking leaf-vein engraved soft and elastic membrane promotes vascular reconstruction

Jinghan Fang, Huaqian Liu, Wei Qiao, Tianpeng Xu, Yuhe Yang, Huizhi Xie, Chun-Hei Lam, Kelvin W. K. Yeung, Xin Zhao**

Jinghan Fang, Huizhi Xie, Prof. Kelvin W. K. Yeung
Department of Orthopaedics and Traumatology, Li Ka Shing Faculty of Medicine, The University of Hong Kong, Hong Kong SAR, China
E-mail: wkkyeung@hku.hk

Huaqian Liu, Tianpeng Xu, Dr. Yuhe Yang, Chun-Hei Lam, Dr. Xin Zhao
Department of Biomedical Engineering, The Hong Kong Polytechnic University, Hong Kong SAR, China
E-mail: xin.zhao@polyu.edu.hk

Dr. Wei Qiao
Faculty of Dentistry, The University of Hong Kong, Hong Kong SAR, China

*Corresponding author

Abstract

Hierarchical vasculature reconstruction is fundamental for tissue regeneration. The regeneration of functional vascular network requires a proper directional guidance, especially in case of large-size defects. To provide the "running track" for vasculature, we developed a leaf-vein-mimetic membrane using soft and elastic poly (lactide-co-propylene glycol-co-lactide) dimethacrylate (PGLADMA). Engraved with an interconnected and perfusable leaf-vein micropattern, the membrane could guide human umbilical vein endothelial cells (HUVECs) to form vasculature *in vitro*. In particular, the "running track" upregulated the angiogenesis-related gene expression and promoted the HUVECs to differentiate into tip cells and stalk cells via tuning vascular endothelial growth factor receptor 2 (VEGFR2) signaling transduction. As a proof of concept, we evaluated its revascularization capability using a rat calvarial defect model *in vivo*. The *in vivo* results demonstrated that the leaf-vein engraved membrane accelerated the formation and maturation of vasculature, leading to a hierarchical blood vessel network. With the superior pro-vasculature property, we believe that the leaf-vein engraved membrane is not only an ideal candidate for the reconstruction of calvarial vasculature but also a promising solution for more complicated vasculature reconstruction, such as muscle, skin, and heart, etc.

Keywords: microtopography, angiogenesis, leaf vein, poly (lactide-co-propylene glycol-co-lactide) dimethacrylate

1. Introduction

Angiogenesis is fundamental in the process of tissue regeneration, while the insufficient blood supply in defect region leads to necrosis and compromised tissue regeneration.[1, 2] To provide sufficient nutrients to nearby cells (diffusion distance < 200 μm), a hierarchical and branching vasculature is indispensable, since a disorganized structure will inevitably cause hypoxic areas, blood vessel leakiness or unfunctional blood lakes where cellular demands cannot be met.[3] However, although a significant number of studies have been conducted to facilitate faster reconstruction of a vasculature, most of them mainly focus on increasing the blood vessel quantity by incorporation of pro-angiogenic cytokines,[4-7] the reconstruction of functional and hierarchical vascular network remains elusive.[8]

Running tracks help athletes run faster and easier by providing more support with the soft rubber surface and facilitating athletes to run in the correct direction. Similar to athletes, cells also need "running tracks" for better cellular behaviors and functions. The leaf vein is the "vascular system" in plants, which is an evolutionarily optimized network of hierarchical interconnected channels responsible for the exchange of nutrition and waste.[9-11] In addition, as a highly efficient system, leaf vein facilitates high-speed fluid transport with minimum waste of energy.[12] Meanwhile, vascular endothelial cells are mechanosensitive cells whose behavior can also be regulated by physical cues.[13] We therefore believe that a leaf vein system built on a suitable foundation matrix is a promising approach for the reconstruction of a functional vascular network.

Here, we design a leaf-vein engraved soft and elastic membrane for the reconstruction of a vascular network **(Figure 1)**. We use the photocrosslinkable, soft and elastic poly (lactide-co-propylene glycol-co-lactide) dimethacrylate (PGLADMA) as the matrix material to build the leaf-vein engraved membrane due to its tunable mechanical property, favorable cytocompatibility, and capability in producing complicated and delicate micropatterns.[14-16] We prepare the leaf-vein engraved membrane using PGLADMA by cast molding using a silicon wafer mold with leaf-vein-micropatterns. We find that the leaf-vein engraved membrane can induce human umbilical vein endothelial cells (HUVECs) to form vasculature *in vitro* and *in vivo*, with increased migration capacity and upregulated angiogenesis-related gene expression. As a proof of concept, we use rat calvarial defects as an animal model to demonstrate the efficacy of the leaf-vein engraved membrane in angiogenesis. The *in vivo* results using a rat calvarial defect model show that the leaf-vein engraved membrane accelerates the formation and maturation of vasculature, achieving a hierarchical blood vessel network.

This vasculature reconstruction process is solely dependent on physical cues without additional biological stimulation (e.g., growth factor addition), circumventing the problem of uncontrollable release of drugs/cytokines, the viability and ethical issues of live cells and tissues, and the high cost and short shelf-life of biological stimuli. We envision that the leaf-vein engraved membrane can not only be a promising candidate for reconstructing vasculature in calvarial defect, but can also provide a new strategy for complicated vasculature reconstruction in multiple tissues, such as muscle, skin, and heart. As a microtopography-based strategy, the

implementation of the leaf-vein engraved membrane can also lay the groundwork for future biomimetic material development and clinical translation.

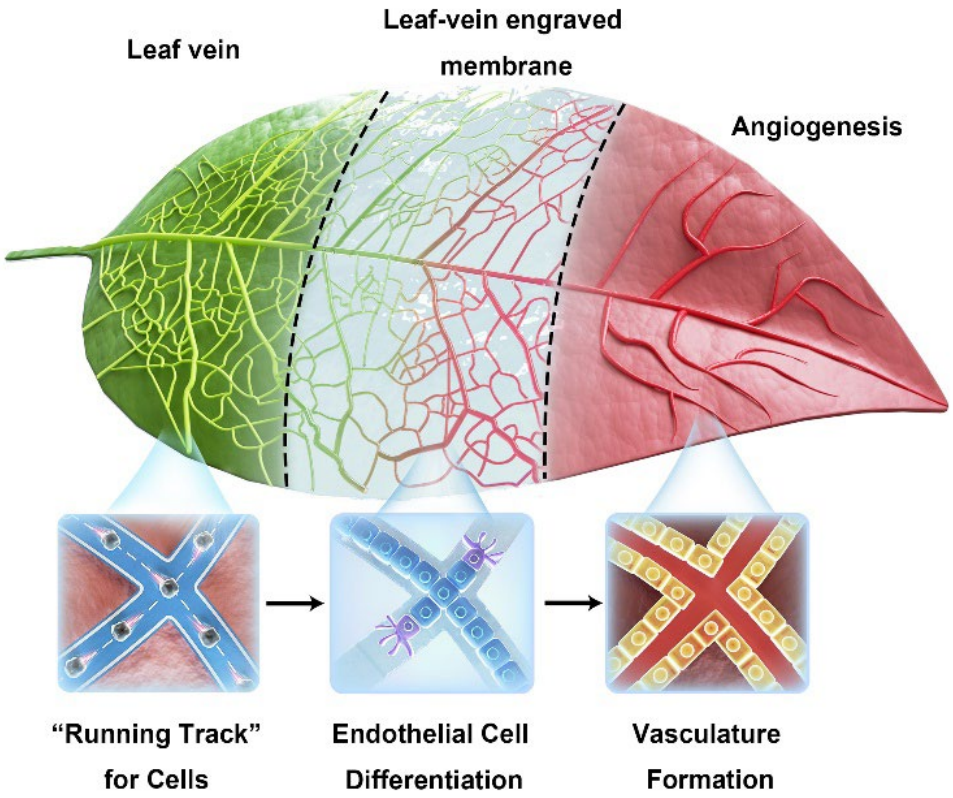

Figure 1. Schematic illustration of the leaf-vein engraved membrane for guiding vasculature formation. Leaf-vein micropatterns is engraved on a PGLADMA polymer membrane, serving as "running tracks" for endothelial cells. The leaf-vein engraved membrane can induce endothelial cell differentiation and subsequent vasculature formation.

2. Results and discussion

2.1 Fabrication of the leaf-vein engraved membrane

In this study, we synthesized a series of photocrosslinkable polymer, PG_mLA_nDMA, where 'm' refers to the unit length of propylene glycol (PPG), and 'n' refers to the molar ratio of lactide (LA) to PPG. We prepared three PGLADMAs with different chain length of PPG and LA blocks: PG_7LA_2DMA, $PG_{17}LA_4DMA$ and $PG_{34}LA_8DMA$ with molecular weights of PPG at 425 (m=7) 1000 (m =17), 2000 (m =34) g/mol, and LA-to-PPG ratios at 2 (n = 2), 4 (n = 4) and 8 (n = 8), respectively. We used $PG_{17}LA_4DMA$, a PGLADMA polymer that has suitable stiffness and flexibility, as the matrix material to fabricate the leaf-vein engraved membrane as depicted in the diagram (**Figure 2A**). The successful synthesis of $PG_{17}LA_4DMA$ was confirmed by ^1H Nuclear magnetic resonance (NMR) and Fourier transform infrared spectroscopy (FTIR). The peaks in the double bond region (~5.6 ppm and ~6.21 ppm) in the ^1H NMR spectrum (Figure 2B), and the peak at 1640 cm^{-1} in the FTIR spectrum indicated the formation of a carbon-carbon

double bond (Figure 2C). We also confirmed the biocompatibility of $PG_{17}LA_4DMA$ using HUVECs by live/dead staining (Figure 2D). MTT results demonstrated that $PG_{17}LA_4DMA$ could favorably support the survival and proliferation of HUVECs (**Figure S1**). The tensile stress-strain curves showed that the $PG_{17}LA_4DMA$ was soft and elastic (Figure 2E): the $PG_{17}LA_4DMA$ was softer than PG_7LA_2DMA (2.48 ± 0.48 MPa), and the stretching performance was better than $PG_{34}LA_8DMA$ (0.08 ± 0.03 MPa) (**Figure S2-3**). The Young's modulus of $PG_{17}LA_4DMA$ (1.06 ± 0.33 MPa) was close to that of soft elastin fibers (0.3-1 MPa), the fibers that dominate the vascular response under physiological blood pressure,[17] suggesting $PG_{17}LA_4DMA$ as a suitable matrix for the regeneration of vasculature. We then prepared the leaf-vein engraved membrane using a silicon wafer mold by means of cast molding as illustrated in the diagram (Figure 2A). After solidification by UV exposure, the leaf-vein engraved membrane was gently peeled off from the mold. We then characterized the geometric structure of the leaf-vein engraved membrane using a stereomicroscope. As shown in Figure 2F-G, delicate leaf-vein channels were carved in the membrane. When perfused with blue ink, the leaf vein in the membrane showed good interconnectivity (Figure 2H). The leaf-vein engraving did not affect the mechanical properties of the membrane (**Figure S4**), and the leaf-vein engraved membrane showed excellent flexibility (**Figure S5**).

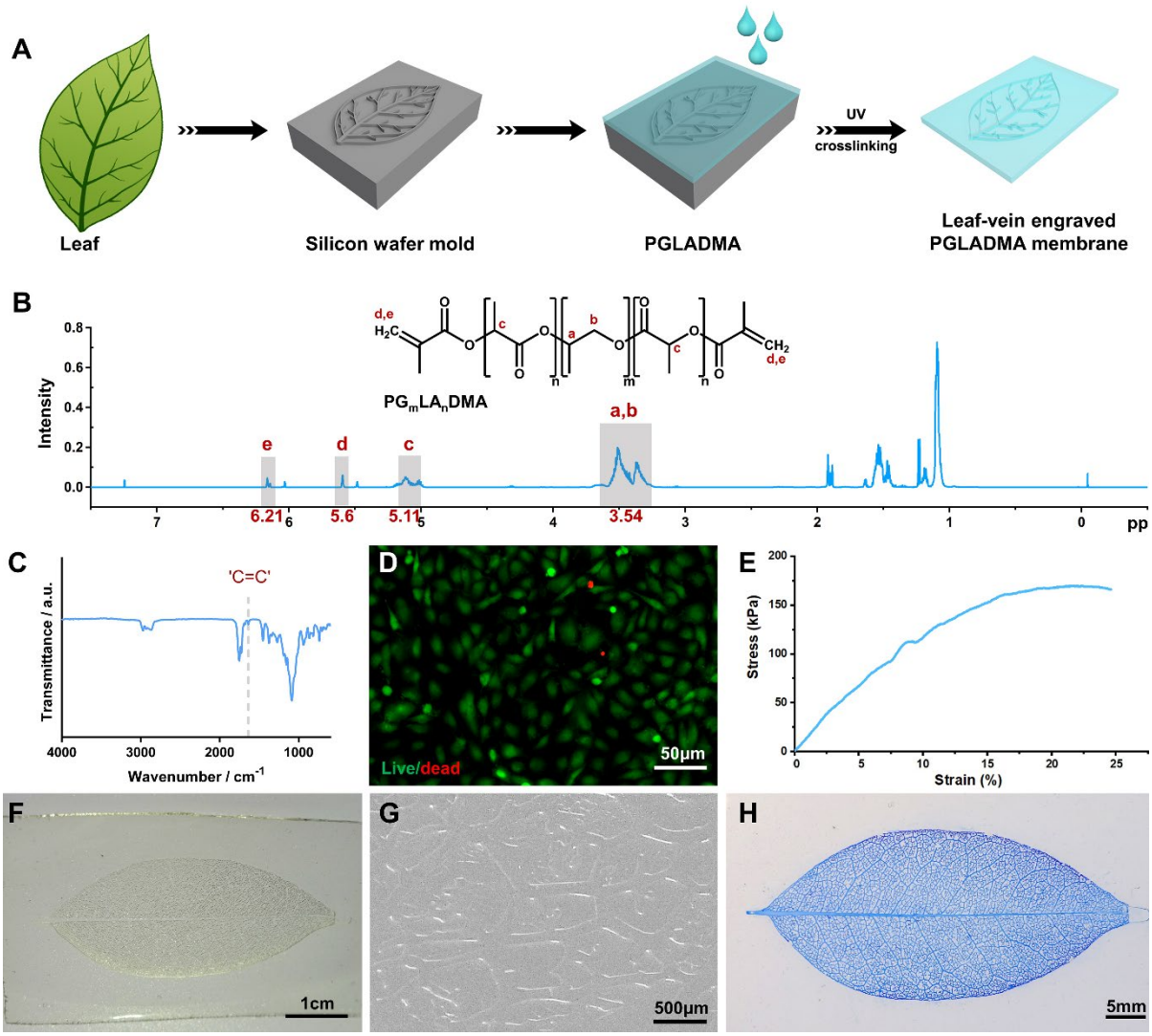

Figure 2. Preparation and characterization of the leaf-vein engraved membrane. (A) Diagram depicting the fabrication process of the leaf-vein engraved membrane. (B) The ^{1}H NMR spectrum of PGLADMA. (C) The FTIR spectrum of $PG_{17}LA_4DMA$. (D) The Live/Dead staining of HUVECs cultured on $PG_{17}LA_4DMA$ for 72 hours. (E) The tensile stress-strain curve of $PG_{17}LA_4DMA$. (F-G) Representative images of leaf-vein engraved membrane. (H) The leaf-vein micropatterns showed good interconnectivity after perfusion with blue ink.

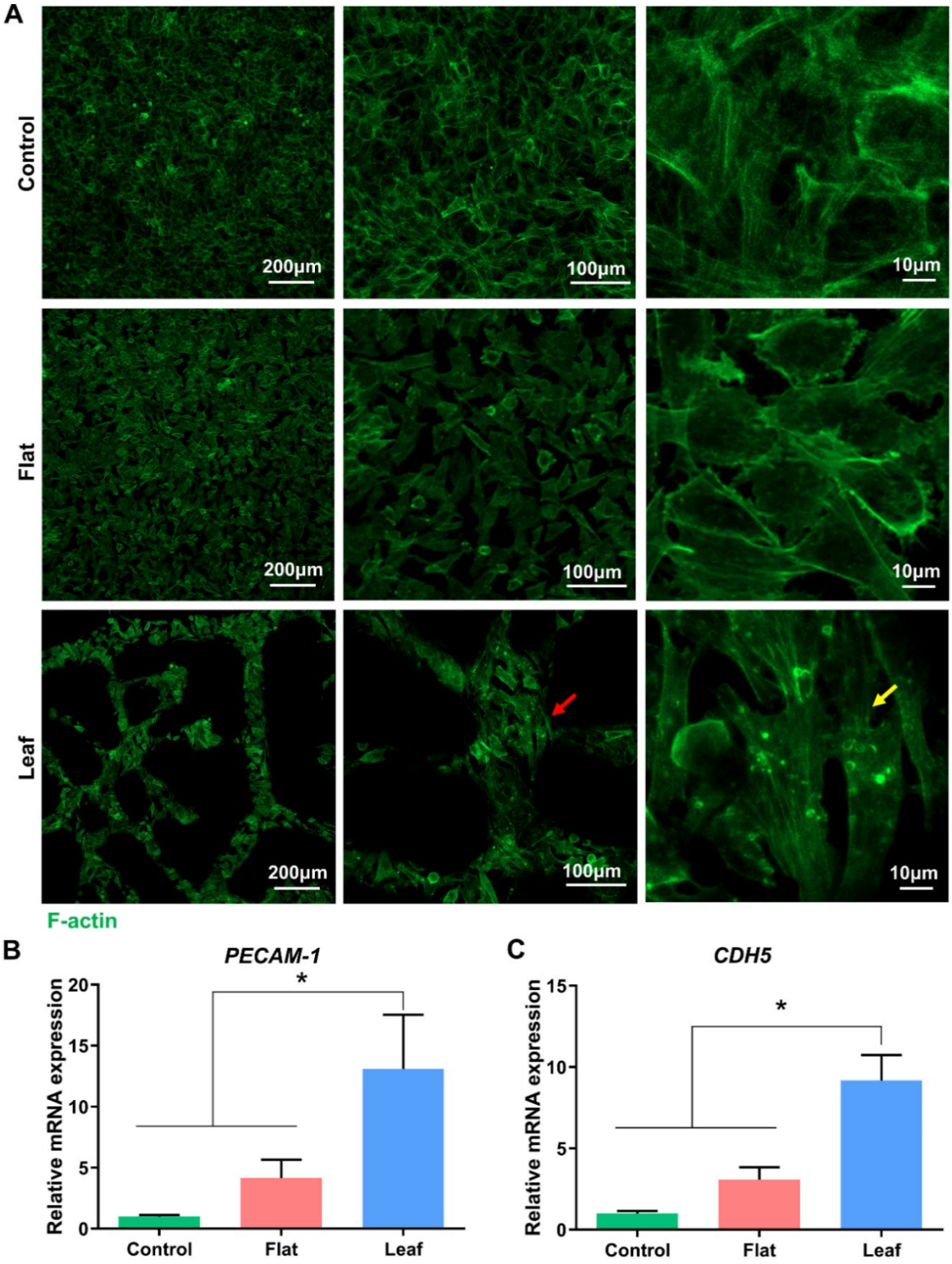

Figure 3. Leaf-vein engraved membrane promoted angiogenesis *in vitro*. (A) The morphology of HUVECs after culture in tissue culture plate, flat membrane and leaf-vein engraved membrane for 72 hours. HUVECs in leaf group showed elongated morphology (red arrows) with long protrusions (yellow arrow). (B, C) The expression of angiogenesis-related genes after 24-hour culture, detected by RT-qPCR (n=3). Error bars represent mean ± SD. * indicated statistically significant difference by one-way ANOVA with Tukey's post hoc test (P<0.05).

2.2 *In vitro* angiogenesis of the leaf-vein engraved membrane

To study whether endothelial cells can form vascular-like structure in the leaf-vein mimetic channels, we cultured HUVECs in the leaf-vein engraved membrane for 3 days. We then stained the F-actin cytoskeleton of the cells with phalloidin to show the cell morphology and cellular alignment **(Figure 3A)**. The HUVECs were observed accumulating in the leaf-vein channels **(Figure S6)**, while HUVECs seeded on flat membrane or tissue culture plate were distributed randomly and showed no signs of vascular network reconstruction (Figure 3A). The 3D reconstruction video showed that the cells formed a vascular-like structure within the leaf vein micropatterns **(Supplementary Video)**. Unlike the polygonal shape in the other two groups, the cells in leaf group have an elongated shape (Figure 3A, red arrow) with long protrusions (Figure 3A, yellow arrow), indicating dynamic cell migration. As the diameter of channel decreased, the cell morphology gradually elongated (**Figure S7**). The RT-qPCR results confirmed that the gene expression of two angiogenic markers, *Platelet and Endothelial Cell Adhesion Molecule 1* (*PECAM-1/CD31*) and *Cadherin 5* (*CDH5*/*VE-cadherin*) were upregulated in the leaf group (Figure 3B-C), suggesting enhanced endothelial cell differentiation and angiogenesis.

Time-lapse live cell tracking of HUVECs demonstrated an enhanced migration of HUVECs by leaf-vein engraved membrane. As depicted in **Figure 4A**, some of the HUVECs in leaf group migrated along the leaf-vein channels and had a longer migration path, while most of the HUVECs in the control and flat group had a random and shorter migration path. Quantitative analysis demonstrated the HUVECs in the leaf group migrated farther and faster than their counterparts, with an overall longer accumulated distance (Figure 4B) and an overall higher mean velocity (Figure 4D). However, when vessels are forming new sprouting, only the leading endothelial cells show higher migration capacity, termed as tip cells, and they only represent a small portion of the endothelial cells.[18, 19] The differentiation and activation of tip cells will also induce the nearby cells differentiate towards stalk cells,[20, 21] the endothelial cells following tip cells. It has been reported that stalk cells have lower migration capacity but are essential to maintain the link between the new sprouting and the original vessels.[20] In line with this, we found that some cells in the leaf group had low accumulated distance and mean velocity (Figure 4B, D). Together, our data indicated that the HUVECs cultured in leaf-vein engraved membrane underwent differentiation into tip cells and stalk cells.

To evaluate the effect of leaf-vein engraved membrane on tip/stalk cell differentiation, we carried out RT-qPCR on HUVECs cultured in control, flat, and leaf group for 24 hours. The gene expression of *KDR*, which encoded vascular endothelial growth factor receptor 2 (VEGFR2), was upregulated in leaf group in comparison with the control and flat group (Figure 4E). As one of the major tip cell markers, *KDR* upregulation was associated with VEGF signaling, the capability of becoming tip cells, and endothelial cell behaviors including survival, proliferation, and migration.[19, 22] However, the gene expression of another tip cell marker, *Dll4*, was not upregulated in leaf group (Figure 4F), suggesting the principal mediator for tip cell differentiation in leaf-vein engraved membrane is VEGFR2. We then evaluated the expression

of stalk cell marker genes. *FLT1*, the gene encoding VEGFR1, was significantly upregulated in the leaf group, compared with the control and the flat group (Figure 4G). The upregulated gene expression of *HEY1*, *JAG1*, and *RHOQ* in the flat and leaf group (Figure 4H-J) suggested that $PG_{17}LA_4DMA$ could support endothelial cell differentiation, and thus was an ideal matrix as a running track for building a functional vascular network. Therefore, the leaf-vein pattern engraved in the soft and elastic polymer membrane enhanced the vascular network formation of endothelial cells by directly promoting endothelial cell differentiation towards tip cell and stalk cells.

To further investigate the biomechanical effects of the leaf-vein micropattern, we prepared simple groove channels in PGLADMA membrane to mimic the smallest to the largest diameter of the channels within the leaf-vein engraved membrane. The depth of the grooves and the leaf-vein micropattern is 70 μm, and diameters of the grooves are: 30 μm, 60 μm, 100 μm, and 150 μm. The RT-qPCR results showed that gene expression of angiogenic marker genes (*PECAM-1*, *CDH5*, **Figure S8 A-B**) and tip cell-related genes (*KDR*, *Dll4*, Figure S8 C-D) displayed an increasing tendency as the channels became narrower, while the gene expression in the leaf group was the highest among all groups. In terms of the stalk cell-related genes, the expression of *FLT1* also displayed a similar tendency as the tip cell related genes (Figure S8 E); while *HEY1, JAG1* and *RHOQ* did not show significant correlation with the channel diameters (Figure S8 F-H). In summary, leaf-vein micropattern is an evolutionarily optimized system with high angiogenic potential, and its function could not be simulated by simple arrangement of microfluidic channels; channels of different diameters may contribute to the regulation of angiogenesis and tip cell/stalk cell differentiation.

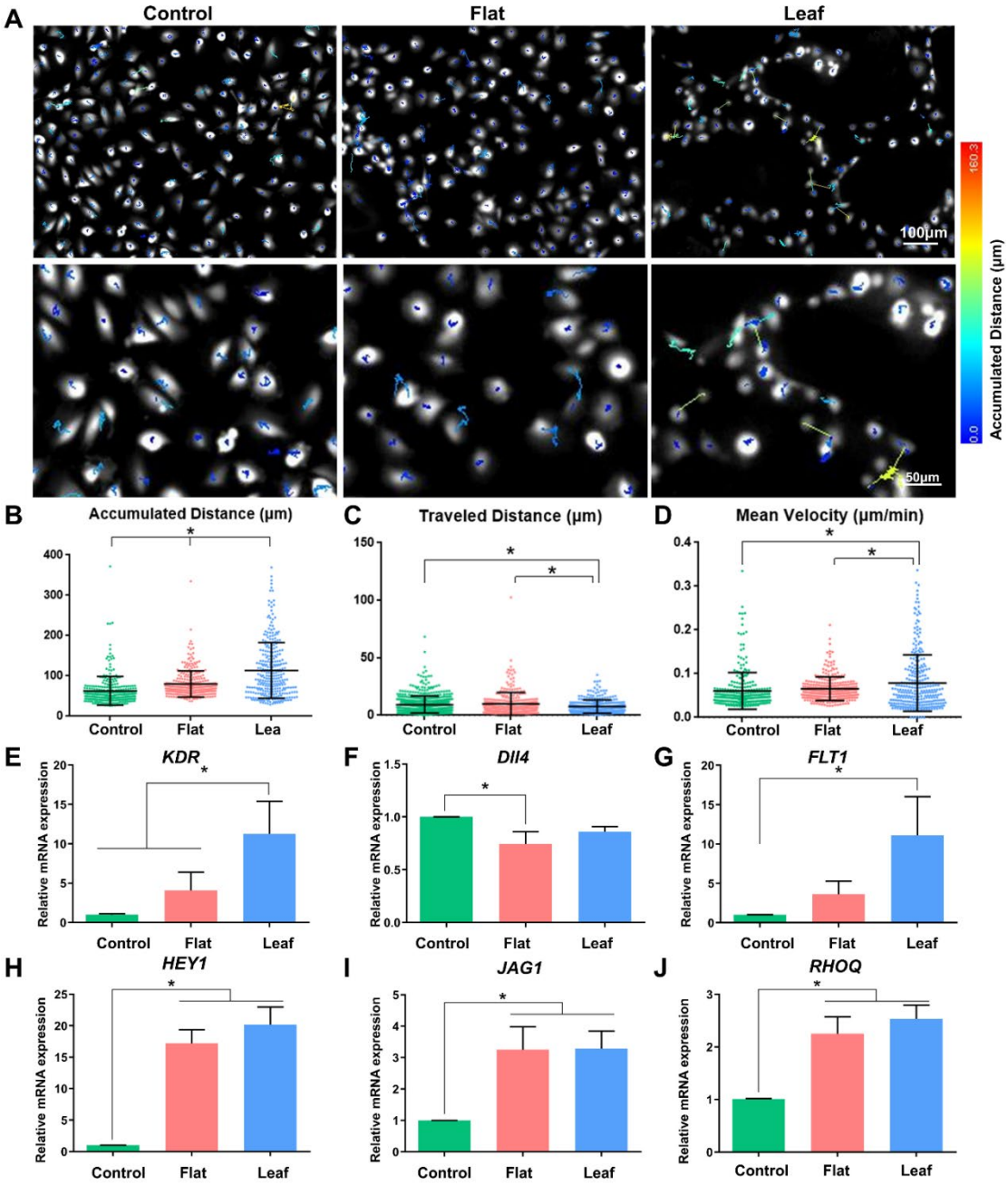

Figure 4. Leaf-vein engraved membrane enhanced endothelial cell differentiation. (A) Cell tracks of HUVECs seeded in tissue culture plate, flat membrane and leaf-vein engraved membrane for 19 hours. The quantification of the accumulated migration distance during the period studied (B), traveled distance between the first location to the last location (C), mean velocity of migrating cells (D) (n=300). (E-J) The expression of tip cell and stalk cell-related genes after 24-hour culture, detected by RT-qPCR (n=3). Error bars represent mean ± SD. * indicated statistically significant difference by one-way ANOVA with Tukey's post hoc test (P<0.05).

2.3 Mechanism of the angiogenesis of the leaf-vein engraved membrane

We then sought to investigate the plausible molecular mechanisms by transcriptome analysis. The differentially expressed genes (DEG) between the control and leaf groups were displayed by volcano plot, with 2980 upregulated and 3069 downregulated genes **(Figure 5A)**. The upregulated DEGs in VEGF signaling pathway (tip cell differentiation) and Notch signaling pathway (stalk cell differentiation) were shown in heatmap (Figure 5B-C), further verifying that the leaf-vein engraved membrane promoted angiogenesis through tip/stalk cell differentiation. Since the upregulated VEGF signaling in tip cells induced the nearby cells differentiate towards stalk cells,[20] VEGF signaling was the critical driving force in endothelial differentiation, and VEGFR2 was found to be the principal receptor for VEGF signaling. Additionally, the cell membrane could function as a mechanosensor and transducer under certain conditions, such as shear stress, where the lipid order of cell membrane and the location of lipid raft, a cholesterol-rich "signaling platform" region in cell membrane, changed accordingly.[23] VEGFR2 was colocalized with caveolin-1 (CAV1) in lipid raft, where Cav-1 stabilized VEGFR2 and kept it in quiescent state.[24] Upon specific stimulations such as VEGFA, VEGFR2 was released from lipid raft and facilitated its phosphorylation and downstream signaling transduction, while the disruption of lipid raft suppressed VEGF signaling.[24] Our data showed that the gene expression of *CAV1* declined in leaf group (Figure 5G), suggesting that the VEGFR2 signaling may be regulated by mechanical microenvironment of the leaf-vein engraved membrane through lipid raft in leaf group.

Next, we performed GO analysis on all upregulated DEGs and plotted the top 20 enriched terms in cellular component (Figure 5D), molecular function **(Figure S9A)**, and biological process (Figure S9B). DEGs (cellular components and molecular function) were enriched in the regulation of cell membrane, cytoplasm, cytoskeleton, and cell projection. These genes were associated with the cell morphology and migration, in accordance with our previous observations on endothelial cell morphological change and migration behavior when cultured in leaf-vein engraved membrane (Figure 3-4). Genes involved in cellular components associated with endocytosis, e.g., endosome, lysosome, cytoplasmic vesicle, and clathrin-coated vesicle, were also enriched. This correlated with the VEGFR2 signaling transduction, which entailed receptor mediated endocytosis, degradation of 40% VEGFR2 by lysosome, and recycling of 60% VEGFR2 to cell membrane.[25] Upregulated *KDR* expression (Figure 4E) suggested increased VEGFR2 protein synthesis in leaf group, which explained the enriched genes in terms of endoplasmic reticulum, Golgi apparatus, and protein transport.

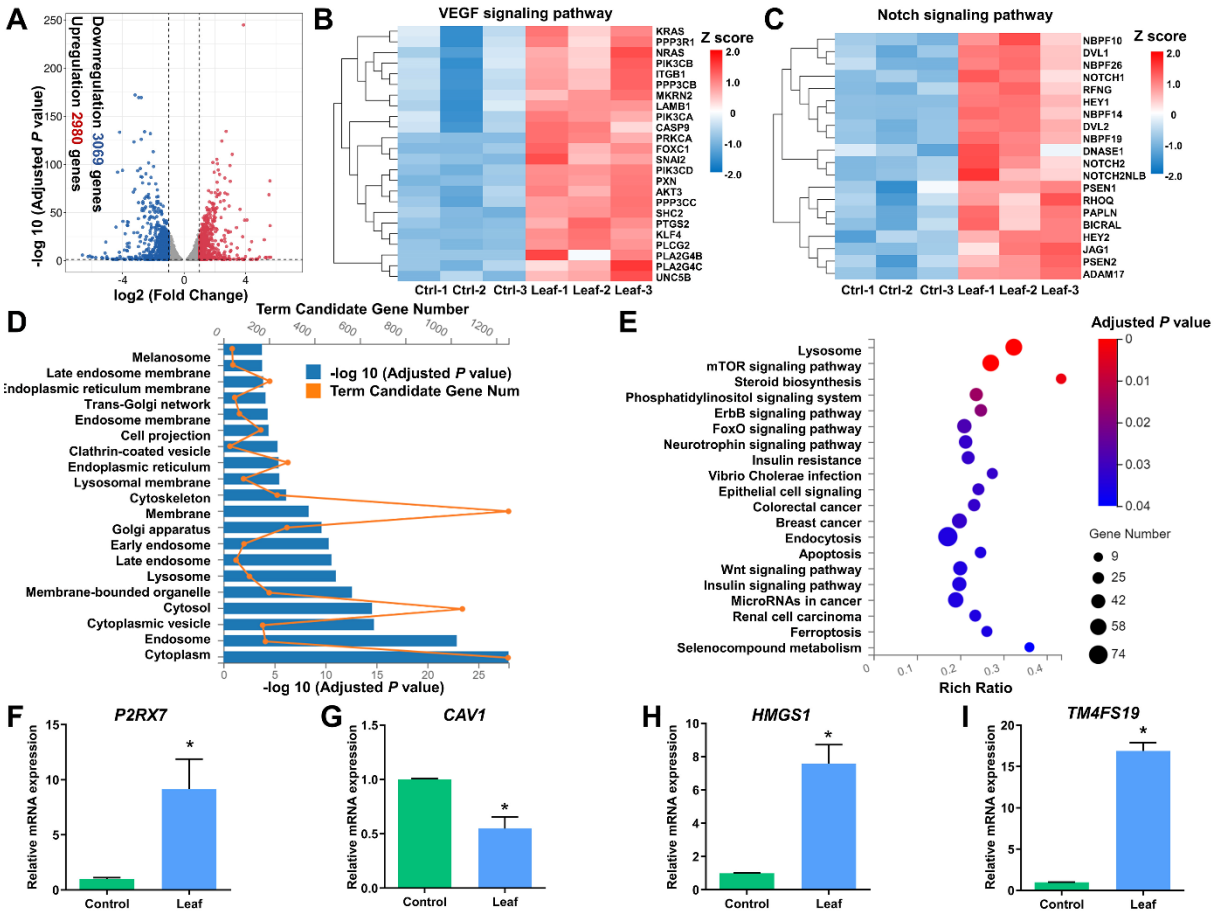

Figure 5. Leaf-vein engraved membrane enhanced tip/stalk cell differentiation through VEGFR2 transduction. Volcano plot (A), heatmap of the DEG in VEGF (B) and Notch (C) signaling pathway. GO enrichment analysis (cellular component) (D), and KEGG pathway enrichment analysis (E) of the upregulated DEG in transcriptome analysis between the control and the leaf group (n=3). (F-I) RT-qPCR validation of the selected genes upregulated in enriched pathways (n=3). Error bars represent mean ± SD. * indicated statistically significant difference by two-sample *t*-test ($P<0.05$).

KEGG analysis results further suggested that endocytosis and mTOR signaling pathway were involved in the endothelial differentiation triggered by the leaf-vein engraved membrane (Figure 5E). As one of the most widely documented angiogenesis-associated pathways,[26, 27] mTOR signaling pathway regulated endothelial cell proliferation, migration and sprouting,[26] and it was reported to be VEGF downstream pathway.[28] To validate the sequencing results, we chose four critical DEGs that were involved in the enriched pathways from the previous volcano plot and performed RT-qPCR (Figure 5F-I). The RT-qPCR validation results on mTOR downstream gene (*P2RX7*),[27] VEGFR2 stabilizer in lipid raft (*CAV1*),[24] cholesterol hemostasis regulator (*HMGCS1*),[29] and endothelial intercellular mediator (*TM4SF19*)[30] confirmed the involvement of the pathways discussed above.

Taken together, the mRNA sequencing results suggested that the leaf-vein engraved membrane promoted angiogenesis via tuning VEGFR2 signal transduction. The leaf-vein

engraved membrane caused cell membrane rearrangement and released VEGFR2 from lipid raft, facilitating VEGFR2 activation, the subsequent endocytosis-mediated signal transduction and recycling of VEGFR2. Activated VEGFR2 promoted mTOR signaling pathway and upregulated the expression of VEGF downstream genes, including the VEGFR2 encoding gene *KDR*. On one hand, the enhanced VEGF signaling induced endothelial cells to differentiate towards tip cells and form new sprouting. On the other hand, upregulated VEGF signaling caused the activation of Notch signaling in nearby endothelial cells, turning them into stalk cells and stabilizing the junction between new sprouting and the original vessel. With VEGF and Notch signaling coordinating with each other, the leaf-vein engraved membrane promoted angiogenesis.

2.4 Angiogenesis efficacy of leaf-vein engraved membrane *in vivo*

We further tested the angiogenic efficacy of different membranes using a rat calvarial defect model (n=3 for each group) at 2 weeks after surgery, a critical timepoint for vascularization quantification.[31] Due to its feasibility in evaluating 3D materials and materials with micropatterns,[15, 32, 33] rat calvarial defect model is a better choice to evaluate the angiogenic capacity of the leaf-vein engraved membrane than conventional angiogenic animal models (e.g., sponge implant model, Matrigel plug assay, chick chorioallantoic membrane, and dorsal skin chamber model), which are more suitable in examining 2D materials or cytokine releasing materials.[34-36]

The H&E staining results showed that most of the vessels in control and flat group were dilated, some of which resembled the morphology of blood lake, while the vessels in leaf group displayed hierarchical distribution **(Figure 6A)**. The angiogenesis process involved sprouting and the subsequent maturation. As vessel maturation was signified by the coverage of pericytes around the endothelial cells to stabilize the nascent vessels,[37] we used a common endothelial cell marker, CD31, and a widely accepted pericyte marker, α-smooth muscle actin (α-SMA), to visualize vessels and mature vessels, respectively.[3] The immunohistochemical staining results confirmed the increased CD31-positive and α-SMA-positive vessels in leaf group in comparison with blank and flat group (Figure 6B). The semi-quantification results on the immunohistochemical staining images showed that the quantity of CD31-positive vessels in leaf group was significantly higher than the flat group (Figure 6C). In accordance with this, the area of vessels in the leaf group was higher than the other two groups (Figure 6D). Moreover, the mature vessel density in leaf group was dramatically higher than blank and flat group (Figure 6E). These results suggested that the leaf-vein engraved membrane accelerated the angiogenesis *in vivo*, with abundant sprouting, speedy vessel maturation, and hierarchical vasculature establishment.

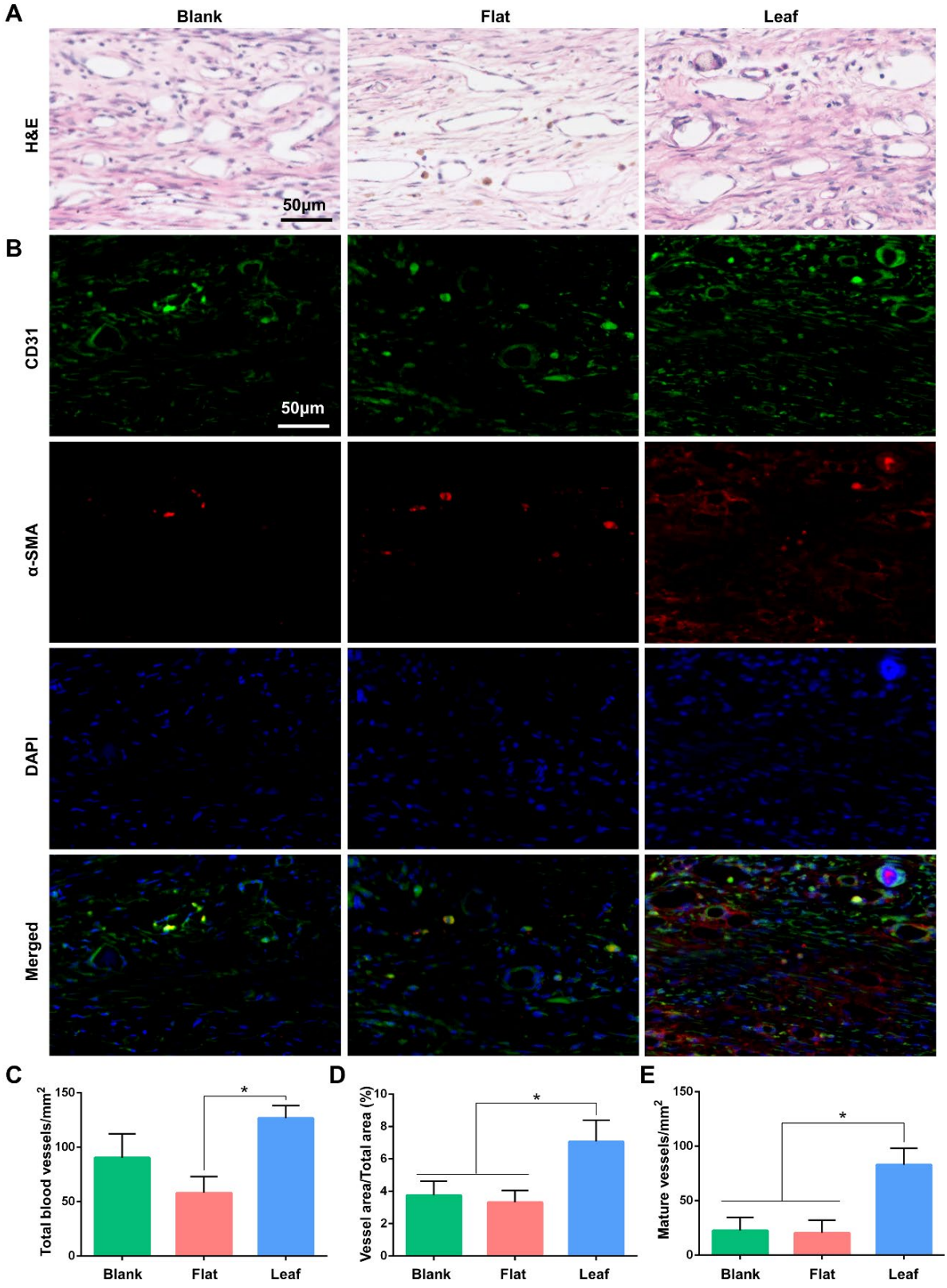

Figure 6. Leaf-vein engraved membrane promoted hierarchical blood vessel formation *in vivo*. (A) Representative H&E images showing the new blood vessel formation in calvarial defects. (B-E) Representative immunofluorescent images and quantification of blood vessels (n=3). Error bars represent mean ± SD. * indicated statistically significant difference by one-way ANOVA with Tukey's post hoc test (P<0.05).

The major function of blood vessels is blood transportation, disorganized vasculature or defective blood vessel walls will cause blood vessel leakiness and impaired blood transportation.[3] In this context, we studied the function of blood vessels by evaluating the deposition of hemosiderin, a sign of chronic hemorrhage,[38] in different groups. In H&E staining images, hemosiderin was brown, yellow particle **(Figure 7A)**, while in Prussian blue staining images, hemosiderin was stained blue (Figure 7B). In blank and flat group, groups of hemosiderin-containing cells were observed within the defect (Figure 7B, arrows). In striking contrast, cells containing hemosiderin was hardly seen in the leaf group (Figure 7B). The semi-quantification results further confirmed the significant lower level of hemosiderin-containing cells in the leaf group in comparison with the blank and flat group (Figure 7C). These indicated that the newly formed vessels in the leaf group were more mature and functional, while the vascularization in the blank and the flat group were immature and leaky. To sum up, the leaf-vein engraved membrane accelerated the formation and maturation of a hierarchical vascular network.

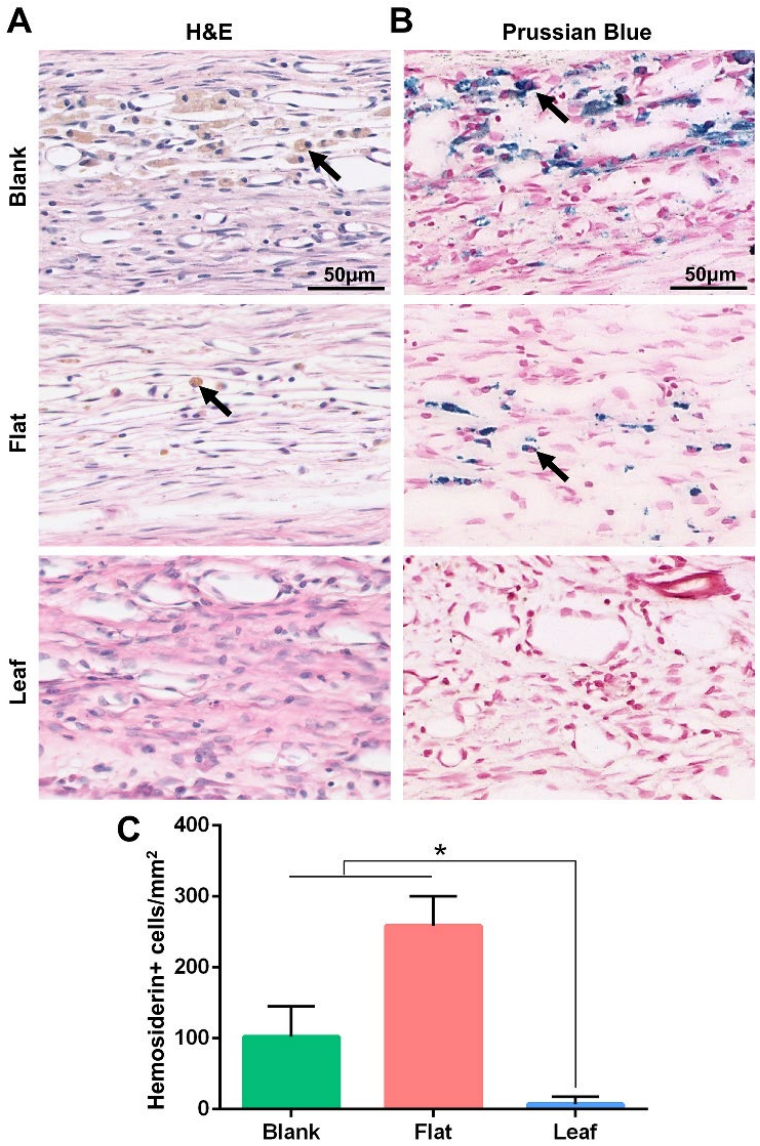

Figure 7. Blood vessels promoted by leaf-vein engraved membrane had little leakiness *in vivo*. (A) Representative H&E images showing the distribution of hemosiderin-containing cells (arrows) in calvarial defects. (B-C) Representative Prussian Blue images and quantification (n=3) of hemosiderin-containing cells (arrows). Error bars represent mean ± SD. * indicated statistically significant difference by one-way ANOVA with Tukey's post hoc test (P<0.05).

3. Conclusion

In summary, we developed a leaf-vein engraved soft and elastic membrane made of photocrosslinkable PGLADMA for the reconstruction of vascular network. The leaf-vein micropatterns in the membrane were interconnected and perfusable for the guidance of vasculature network formation. It stimulated the vasculature formation and migration of HUVECs cells *in vitro* by directly inducing tip/stalk cell differentiation via the VEGFR2 signaling transduction. Moreover, it accelerated the formation and maturation of vascular network *in vivo*, with more hierarchical vascular structure, increased $CD31^+$ α-SMA^+ mature blood vessels and lower level of blood vessel leakiness. By relying solely on physical cues,

leaf-vein micropatterns not only offer an economic and efficient approach to accelerate the vasculature reconstruction, but also avoid the problems posed by biological stimulations, including uncontrollable release of drugs/cytokines, the viability and ethical issues of living cells and tissues. As a microtopography-based strategy, the leaf-vein engraved membrane can offer a novel biomimetic option for reconstruction of tissues with complicated vasculature, such as muscle, skin, and heart, etc.

4. Experimental Section

4.1 Synthesis and characterization of PGLADMA

The photocrosslinkable polymer, PGLADMA, was synthesized as previously documented.[14-16] Briefly, 90g lactide-co-propylene glycol-co-lactide was synthesized from 57 g propylene glycol (molecular weight: 1000, Macklin Reagent, China) and 32.83g lactide (Macklin Reagent, China). The propylene glycol and lactide reacted under nitrogen protection with continuous stirring at 150°C for 6 hours, with stannous octoate (Macklin Reagent, China) as the catalyst. Next, the product reacted with 22.33g methacryloyl chloride (Macklin Reagent, China) and 23.14g trimethylamine (Macklin Reagent, China) at 0°C to produce PGLADMA. The resultant liquid PGLADMA was purified with filtration and characterized using ^{1}H Nuclear magnetic resonance (NMR, JOEL, Japan) and Fourier transform infrared spectroscopy (FTIR) (Thermo Nicolet iS5, USA) as described previously.[14-16]

To solidify the photocrosslinkable PGLADMA, it was first mixed with 10% Irgacure 819 (dissolved in hydroxyethyl methacrylate (Sigma-Aldrich, USA)) at a ratio of 10:1 (v/w). The photocrosslinkable polymer solution in a silicon wafer mold was then vacuumed for 15 minutes and solidified after being exposed to ultraviolet (UV) light (wavelength of 365 nm and intensity of 5 mW/cm^2, Analytikjena, Germany) for 10 minutes. The flexibility evaluation was conducted to intuitively show the bending properties of the PGLADMA membrane. The tensile testing was conducted to characterize the mechanical properties of the flat and leaf-vein PGLADMA membrane (width 65 ± 3 mm, length 38 ± 0.2 mm, thickness 0.5 ± 0.02 mm) on a biaxial testing machine (MTS, US) as previously described.[14] Young's modulus was calculated as illustrated in **Figure S10** using formula (1) by tensile stress-strain test (n=3):

$$E=\frac{Stress\ (\sigma)}{Strain\ (\varepsilon)}=\frac{F/A}{\Delta L/L} \quad (1)$$

The stress (σ) and strain (ε) were acquired by analyzing the PGLADMA materials original length (L, unit: mm), cross-sectional areas (A, unit: mm^2), the force of stretching (F, unit: N) and the linear elastic region (ΔL, unit: mm).

4.2 Preparation and characterization of leaf-vein engraved membrane

The leaf-vein engraved membrane was prepared by cast molding from a silicon wafer mold. The leaf vein of a Mulberry leaf was carved on the silicon wafer mold by photolithography and etching.[39] Next, the precosslinked polymer solution, $PG_{17}LA_4DMA$ with Irgacure 819, was

poured into a silicon wafer mold and then vacuumed for 15 minutes before UV crosslinking for 10 minutes. The crosslinked membrane was gently peeled off from the mold and rinsed with absolute alcohol and deionized water. The air-dried membrane was used for the subsequent experiments. The groove-patterned membranes were prepared by the same method, except for using a silicon wafer mold with grooves (diameter of grooves: 30 μm, 60 μm, 100 μm, and 150 μm).

4.3 Cell viability, proliferation, and morphology assay

HUVECs (ATCC, USA) were maintained in human large vessel endothelial cell basal medium (M200) supplemented with large vessel endothelial supplement (ThermoFisher Scientific, USA) and 1% Penicillin-Streptomycin (Gibco, USA) according to manufacturer's instruction, which was thereafter referred to as HUVEC culture medium.

To test the biocompatibility of the leaf-vein engraved membrane, HUVEC culture medium was added onto the material and was vacuumed for 30 minutes to avoid air trapping in the leaf vein channels. HUVECs were then seeded onto the tissue culture plate (control), flat membrane (flat), and leaf-vein engraved membrane (leaf) at a density of $1.25x10^5$cell/cm^2 and cultured for 3 days. Cell viability was examined using the Live/Dead® Viability/Cytotoxicity Kit (ThermoFisher Scientific, USA). Cell proliferation was examined using the MTT Cell Proliferation Kit (ThermoFisher Scientific, USA). The fluorescent images were captured using a fluorescent microscope (Nikon, Japan) for cell viability quantification.

To examine the cell morphology, the samples were then fixed with 4% paraformaldehyde (Biosharp, China) and rinsed with phosphate buffered saline (PBS, Gibco, USA) twice before permeation for 20 minutes using 0.1% Triton (Sigma-Aldrich, USA). Next, the samples were rinsed with PBS twice and blocked in 3% bovine serum albumin (Sigma-Aldrich, USA) for 1 hour. For F-actin staining, the cells were stained with Alexa Fluor 488-conjugated Phalloidin (ThermoFisher Scientific, USA) at 4°C overnight. The fluorescent images were captured using an LSM 900 confocal microscope (Zeiss, Germany).

4.4 Cell migration tracking

The HUVECs were labeled with CellTracker™ fluorescent probes (ThermoFisher Scientific, USA) according to manufacturer's instruction one day before migration tracking. Before cell seeding, HUVEC culture medium was added onto the material and was vacuumed for 30 minutes to avoid air trapping in the leaf vein channels. For cell tracking, the cells were seeded on tissue culture plate (control), flat membrane (flat), and leaf-vein engraved membrane (leaf) at a density of $3x10^4$ cells/cm^2 and allowed to attach for 5 hours in the incubator before cell migration tracking. The migration of cells was observed by time-lapse microscopy for 19 hours using a Nikon Eclipse Ti2-E widefield microscope (Nikon, Japan) under humid environment with 5% CO_2 at 37°C. The migration paths as well as the quantification of accumulated distance, traveled distance, and mean velocity were analyzed by ImageJ (Fiji) 1.53f51 software (NIH, USA) with a sample size of 300 cells per group.

4.5 PCR and transcriptome sequencing analysis

As described in 4.4, HUVECs were seeded onto the tissue culture plate (control), flat membrane (flat), groove-patterned and leaf-vein engraved membrane (leaf) at a density of $5x10^4$cells/cm^2 and cultured in HUVEC culture medium for 24 hours. After supernatant collection, the cells were rinsed with PBS twice and the leaf-vein engraved membrane was gently scrabbed using a clean tissue culture plate to remove the cells on the flat surface among the channels as well as the surrounding area without pattern, leaving the cells remaining in the leaf vein channels. For the flat group and the control group, all cells were collected. The cells for groove-patterned groups were collected using the same method as the leaf group. The cells were then trypsinized and collected by centrifugation (1,000 rpm, 5 minutes) before RNA extraction. The total RNA was extracted using RNeasy Plus kit (Qiagen, USA) following the manufacturer's instructions. The reverse transcription and the RT-qPCR process was as previously described (n=3 for each group).[40] The primer sequences are listed in **Table 1**. The transcriptome sequencing (n=3 for each group) was performed on MGIseq 2000 (BGI, China). DEG (log2(fold change)$\geqslant$0.25, adjusted *P* value < 0.05) were selected for subsequent analysis. The GO and KEGG pathway enrichment analyses were performed using the free online platform of Dr. Tom (BGI, China).

Table 1. Primers applied for RT-qPCR.

Genes	Primer sequences
PECAM-1	Forward: 5'- AACAGTGTTGACATGAAGAGCC -3'
	Reverse: 5'- TGTAAAACAGCACGTCATCCTT -3'
CDH5	Forward: 5'- AAGCGTGAGTCGCAAGAATG -3'
	Reverse: 5'- TCTCCAGGTTTTCGCCAGTG -3'
KDR	Forward: 5'- GGCCCAATAATCAGAGTGGCA -3'
	Reverse: 5'- CCAGTGTCATTTCCGATCACTTT -3'
Dll4	Forward: 5'- GTCTCCACGCCGGTATTGG -3'
	Reverse: 5'- CAGGTGAAATTGAAGGGCAGT -3'
FLT1	Forward: 5'- TTTGCCTGAAATGGTGAGTAAGG -3'
	Reverse: 5'- TGGTTTGCTTGAGCTGTGTTC -3'
HEY1	Forward: 5'- GTTCGGCTCTAGGTTCCATGT -3'
	Reverse: 5'- CGTCGGCGCTTCTCAATTATTC -3'
JAG1	Forward: 5'- GTCCATGCAGAACGTGAACG -3'
	Reverse: 5'- GCGGGACTGATACTCCTTGA -3'
RHOQ	Forward: 5'- CCACCGTCTTCGACCACTAC -3'
	Reverse: 5'- AGGCTGGATTTACCACCGAGA -3'
P2RX7	Forward: 5'- TATGAGACGAACAAAGTCACTCG -3'
	Reverse: 5'- GCAAAGCAAACGTAGGAAAAGAT -3'
CAV1	Forward: 5'- GCGACCCTAAACACCTCAAC -3'
	Reverse: 5'- ATGCCGTCAAAACTGTGTGTC -3'

HMGS1	Forward: 5'- GATGTGGGAATTGTTGCCCTT -3'
	Reverse: 5'- ATTGTCTCTGTTCCAACTTCCAG -3'
TM4FS19	Forward: 5'- CACGGACTTGCTCCCGTATC -3'
	Reverse: 5'- GCCCCTCAACAGGTAGGTG -3'
GAPDH	Forward: 5'- GGAGCGAGATCCCTCCAAAAT -3'
	Reverse: 5'- GGCTGTTGTCATACTTCTCATGG -3'

4.6 Animal study

The animal experiments were carried out according to a protocol approved by the Committee on the Use of Live Animals in Teaching and Research (CULATR, the University of Hong Kong). Male Sprague Dawley rats aged 9-12 weeks were used (n=3 for each group). Under anesthesia with a combination of xylazine (6 mg/kg) and ketamine (67 mg/kg), a 1.5 cm sagittal incision was made on the scalp of the rats, and the calvarium was exposed by blunt dissection. Two bilateral 5 mm calvarial defects were created using a diameter trephine bur with sufficient saline irrigation. Except for blank control group where no material was implanted, each defect was covered by a piece of flat membrane (flat), or leaf-vein engraved membrane (leaf). After closing the surgical wound with suture, the rats received subcutaneous injection of Oxytetracycline (30 mg/kg), Flunixin (2.5 mg/kg), and Buprenorphine (0.5 mg/kg). The rats were euthanized 2 weeks after surgery, followed by intracardiac perfusion with PBS and 4% paraformaldehyde (PFA). The tissue was harvested and fixed with 4% PFA overnight and decalcified with 10% ethylenediaminetetraacetic acid for subsequent analysis. Haematoxylin and eosin (H&E) staining and immunohistochemical (IHC) staining (Sigma-Aldrich, USA) was performed as described previously.[40] For IHC, the primary antibodies used were anti-CD31 (1:50 dilution, Abcam, USA) and anti-α-SMA (1:29000 dilution, Abcam, USA). Prussian blue staining was performed using a Prussian blue staining kit (Solarbio, China) according to the manufacturer's instructions. Brightfield images were captured using a Vectra Polaris imaging system (Akoya Biosciences, USA). The fluorescent images were captured using a Nikon Eclipse Ti2-E widefield microscope (Nikon, Japan). For semi-quantification, three 20x images were randomly selected from each specimen. The vessel density (total CD31-positive blood vessels per mm^2), ratio of vessel area (CD31-positive) against total area, mature vessel density (CD31-positive, α-SMA-positive blood vessels per mm^2) was calculated by ImageJ (Fiji) 1.53f51 software (NIH, USA) as described previously.[41-43] The cells containing blue granules (indicating hemosiderin when stained with Prussian blue) were calculated for the semi-quantification of hemosiderin.

4.7 Statistical analysis

All data analyses were performed and illustrated using the Prism software (version 6, GraphPad, USA). For comparisons between two groups, two-sample *t*-test was used; for comparisons among multiple groups, one-way analysis of variance (ANOVA) was used, followed by Tukey's multiple-comparison post hoc test. All data are presented as mean ± standard deviation (SD).

The levels of significant difference among the groups were defined and noted as $*P < 0.05$. Each experiment was performed at least three times.

Supporting Information

Supporting Information is available from the Wiley Online Library or from the author.

Acknowledgments: JH Fang and HQ Liu contributed equally to this work. This work was supported by the National Key R&D Program of China (2018YFA0703100), and National Excellent Young Scientists Fund (Hong Kong and Macau, 82122002), National Natural Science Foundation of China.

Conflict of Interest: The authors declare that there is no conflict of interest.

References

[1] C. Fondi, A. Franchi, *Clin. Cases Miner. Bone Metab.*, **2007**, *4,* 21.
[2] O. Tsigkou, I. Pomerantseva, J.A. Spencer, P.A. Redondo, A.R. Hart, E. O'Doherty, Y. Lin, C.C. Friedrich, L. Daheron, C.P. Lin, C.A. Sundback, J.P. Vacanti, C. Neville, *Proc. Natl. Acad. Sci. U. S. A.*, **2010**, *107,* 3311.
[3] D.M. McDonald, P.L. Choyke, *Nat. Med.*, **2003**, *9,* 713.
[4] T. Wang, Y. Zhai, M. Nuzzo, X. Yang, Y. Yang, X. Zhang, *Biomaterials*, **2018**, *182,* 279.
[5] L. Wu, Y. Gu, L. Liu, J. Tang, J. Mao, K. Xi, Z. Jiang, Y. Zhou, Y. Xu, L. Deng, L. Chen, W. Cui, *Biomaterials*, **2020**, *227,* 119555.
[6] R. Shi, J. Zhang, K. Niu, W. Li, N. Jiang, J. Li, Q. Yu, C. Wu, *Biomater. Sci.*, **2021**, *9,* 2090.
[7] G. Yang, H. Liu, Y. Cui, J. Li, X. Zhou, N. Wang, F. Wu, Y. Li, Y. Liu, X. Jiang, S. Zhang, *Biomaterials*, **2021**, *268,* 120561.
[8] R.C. Goncalves, A. Banfi, M.B. Oliveira, J.F. Mano, *Biomaterials*, **2021**, *269,* 120628.
[9] B. Blonder, S. Both, M. Jodra, H. Xu, M. Fricker, I.S. Matos, N. Majalap, D. Burslem, Y.A. Teh, Y. Malhi, *New. Phytol.*, **2020**, *228,* 1796.
[10] A. Roth-Nebelsick, *Ann. Bot.*, **2001**, *87,* 553.
[11] L. Sack, C. Scoffoni, *New. Phytol.*, **2013**, *198,* 983.
[12] M. Mao, J. He, Y. Lu, X. Li, T. Li, W. Zhou, D. Li, *Biofabrication*, **2018**, *10,* 025008.
[13] J.D. Humphrey, *Hypertension*, **2008**, *52,* 195.
[14] Y. Yang, Q. Zhang, T. Xu, H. Zhang, M. Zhang, L. Lu, Y. Hao, J.H. Fuh, X. Zhao, *Biomaterials*, **2020**, *263,* 120378.
[15] Y. Yang, T. Xu, H.P. Bei, Y. Zhao, X. Zhao, *Adv. Funct. Mater.*, **2021**, *31,* 2104636.
[16] X. Zhao, I. Olsen, H. Li, K. Gellynck, P.G. Buxton, J.C. Knowles, V. Salih, A.M. Young, *Acta. Biomater.*, **2010**, *6,* 845.
[17] D.B. Camasao, D. Mantovani, *Mater. Today Bio*, **2021**, *10,* 100106.
[18] R. del Toro, C. Prahst, T. Mathivet, G. Siegfried, J.S. Kaminker, B. Larrivee, C. Breant, A. Duarte, N. Takakura, A. Fukamizu, J. Penninger, A. Eichmann, *Blood*, **2010**, *116,* 4025.
[19] L. Jakobsson, C.A. Franco, K. Bentley, R.T. Collins, B. Ponsioen, I.M. Aspalter, I. Rosewell, M. Busse, G. Thurston, A. Medvinsky, S. Schulte-Merker, H. Gerhardt, *Nat. Cell. Biol.*, **2010**, *12,* 943.

[20] R. Blanco, H. Gerhardt, *Cold Spring Harb. Perspect. Med.*, **2013**, *3,* a006569.
[21] C. Margadant, *Angiogenesis*, **2020**, *23,* 75.
[22] A. Benn, C. Hiepen, M. Osterland, C. Schutte, A. Zwijsen, P. Knaus, *FASEB J.*, **2017**, *31,* 4720.
[23] K. Yamamoto, J. Ando, *J. Cell. Sci.*, **2013**, *126,* 1227.
[24] A. Laurenzana, G. Fibbi, A. Chilla, G. Margheri, T. Del Rosso, E. Rovida, M. Del Rosso, F. Margheri, *Cell. Mol. Life Sci.*, **2015**, *72,* 1537.
[25] I.O. Zabroski, M.A. Nugent, *Int. J. Mol. Sci.*, **2021**, *22,* 798.
[26] H. Elmasri, E. Ghelfi, C.W. Yu, S. Traphagen, M. Cernadas, H. Cao, G.P. Shi, J. Plutzky, M. Sahin, G. Hotamisligil, S. Cataltepe, *Angiogenesis*, **2012**, *15,* 457.
[27] Y. Zhang, H. Cheng, W. Li, H. Wu, Y. Yang, *Int. J. Cancer.*, **2019**, *145,* 1068.
[28] Q. Xue, J.A. Nagy, E.J. Manseau, T.L. Phung, H.F. Dvorak, L.E. Benjamin, *Arterioscler. Thromb. Vasc. Biol.*, **2009**, *29,* 1172.
[29] X. Ying, Y. Zhu, X. Jin, X. Chang, *Placenta*, **2021**, *103,* 86.
[30] L. Ding, L.M. Li, B. Hu, J.L. Wang, Y.B. Lu, R.Y. Zhang, X. He, C. Shi, L.M. Wu, C.M. Wu, B. Yang, L. Zheng, B.H. Ping, Y.W. Hu, Q. Wang, *Biochem. Biophys. Res. Commun.*, **2020**, *533,* 1204.
[31] Z. Li, C.A. Meyers, L. Chang, S. Lee, Z. Li, R. Tomlinson, A. Hoke, T.L. Clemens, A.W. James, *J. Clin. Invest.*, **2019**, *129,* 5137.
[32] X. Liu, M. Chen, J. Luo, H. Zhao, X. Zhou, Q. Gu, H. Yang, X. Zhu, W. Cui, Q. Shi, *Biomaterials*, **2021**, *276,* 121037.
[33] C. Feng, W. Zhang, C. Deng, G. Li, J. Chang, Z. Zhang, X. Jiang, C. Wu, *Adv. Sci.*, **2017**, *4,* 1700401.
[34] S. Kargozar, F. Baino, S. Hamzehlou, R.G. Hill, M. Mozafari, *Trends. Biotechnol.*, **2018**, *36,* 430.
[35] J. Hasan, S.D. Shnyder, M. Bibby, J.A. Double, R. Bicknel, G.C. Jayson, *Angiogenesis*, **2004**, *7,* 1.
[36] K. Norrby, *J. Cell. Mol. Med.*, **2006**, *10,* 588.
[37] R.K. Jain, *Nat. Med.*, **2003**, *9,* 685.
[38] L.B. Radakovich, C.S. Olver, *Vet. Clin. North Am. Small Anim. Pract.*, **2017**, *47,* 17.
[39] J. He, M. Mao, Y. Liu, J. Shao, Z. Jin, D. Li, *Adv. Healthc. Mater.*, **2013**, *2,* 1108.
[40] W. Qiao, H. Xie, J. Fang, J. Shen, W. Li, D. Shen, J. Wu, S. Wu, X. Liu, Y. Zheng, K.M.C. Cheung, K.W.K. Yeung, *Biomaterials*, **2021**, *276,* 121038.
[41] X. Sun, Q. Lang, H. Zhang, L. Cheng, Y. Zhang, G. Pan, X. Zhao, H. Yang, Y. Zhang, H.A. Santos, W. Cui, *Adv. Funct. Mat.*, **2017**, *27,* 1604617.
[42] R. Xu, A. Yallowitz, A. Qin, Z. Wu, D.Y. Shin, J.M. Kim, S. Debnath, G. Ji, M.P. Bostrom, X. Yang, C. Zhang, H. Dong, P. Kermani, S. Lalani, N. Li, Y. Liu, M.G. Poulos, A. Wach, Y. Zhang, K. Inoue, A. Di Lorenzo, B. Zhao, J.M. Butler, J.H. Shim, L.H. Glimcher, M.B. Greenblatt, *Nat. Med.*, **2018**, *24,* 823.
[43] R. Rust, T. Kirabali, L. Gronnert, B. Dogancay, Y.D.P. Limasale, A. Meinhardt, C. Werner, B. Lavina, L. Kulic, R.M. Nitsch, C. Tackenberg, M.E. Schwab, *Front. Neurosci.*, **2020**, *14,* 244.